Journal of Colloid and Interface Science 603 (2021) 771–782

Contents lists available at ScienceDirect

Journal of Colloid and Interface Science

journal homepage: www.elsevier.com/locate/jcis

Dual-functional biocatalytic membrane containing laccase-embedded metal-organic frameworks for detection and degradation of phenolic pollutant

Dawei Li [a], Yue Cheng [a], Han Zuo [a], Wei Zhang [a], Gangwei Pan [a], Yijun Fu [a,*], Qufu Wei [b,**]

[a] National and Local Joint Engineering Research Center of Technical Fiber Composites for Safety and Health, School of Textile and Clothing, Nantong University, Nantong 226019, China
[b] Key Laboratory of Eco-Textiles, Ministry of Education, Jiangnan University, 1800 Lihu Avenue, Wuxi, Jiangsu Province 214122, PR China

GRAPHICAL ABSTRACT

A novel biocatalytic membrane based on bacterial cellulose (BC), laccase@zeolitic imidazolate framework-90 (LAC@ZIF-90) biocomposites, and carboxylated multi-walled carbon nanotubes (c-MWCNTs) was prepared through a facile method for detection and degradation of phenolic pollutant.

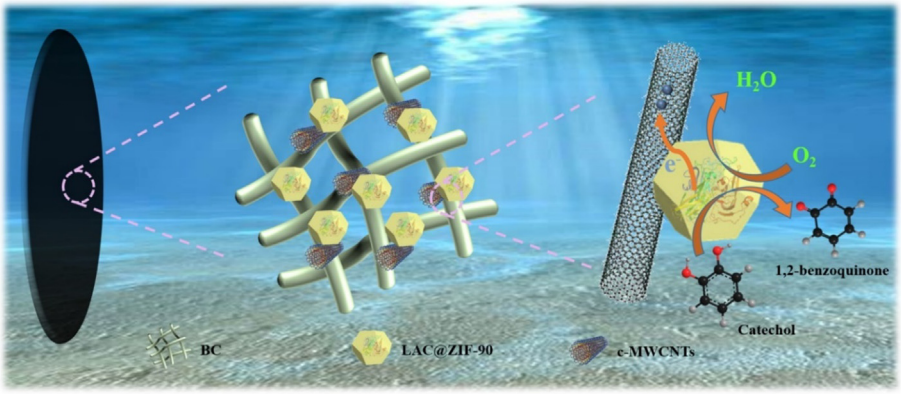

ARTICLE INFO

Article history:
Received 21 May 2021
Revised 17 June 2021
Accepted 27 June 2021
Available online 30 June 2021

Keywords:
Bacterial cellulose
Metal-organic framework
Biocatalytic membrane
Phenolic pollutant
Laccase biosensor

ABSTRACT

In this work, a metal–organic framework material, zeolitic imidazolate framework-90 (ZIF-90), was firstly used to encapsulate laccase (LAC) and to prepare ZIF-90/LAC biocomposites. Afterward, the composites were combined with bacterial cellulose (BC) and carboxylated multi-walled carbon nanotubes (c-MWCNTs) by a facile method to achieve a novel cellulose membrane with biocatalytic function, displaying excellent detection and degradation properties towards phenolic pollutant. Notably, the membrane was directly employed as a biosensor electrode, and it exhibited a linear response to catechol from 20 to 400 μM with a detection limit of 1.86 μM (S/N = 3), as well as satisfactory selectivity, reproducibility, and stability. In addition, the biocatalytic membrane showed higher degradation efficiency towards catechol than pure LAC, and the catechol degradation efficiency of the membrane generally ranged from 93.4% to 82.1% for five cycles. Moreover, the membrane was successfully applied in enzyme membrane reactor (EMR), achieving satisfactory results. The novel membrane harbors a broad application prospect in the fields of real-time monitor and treatment of phenolic wastewater.

* Corresponding author.
** Corresponding author.
E-mail addresses: fuyj@ntu.edu.cn (Y. Fu), qfwei@jiangnan.edu.cn (Q. Wei).

https://doi.org/10.1016/j.jcis.2021.06.155
0021-9797/

1. Introduction

As the rapid development of global economy, environmental problems have attracted increasingly wide attention. Among multitudinous pollutants, waste water containing phenols or phenolic compounds from textiles, dyes, agrochemicals, or packing materials, is not only a great threat to ecosystem, but also hazardous and dangerous to physical health of people [1,2]. Moreover, phenol and phenolic compounds were included as a priority pollutant in the list issued by the United States Environmental Protection Agency (USEPA), requiring that the content of phenol in drinking water must be less than 1 g/L. [3]. Therefore, it is meaningful to exploit methods which can not only detect but also remove phenolic compounds.

Up to now, a variety of methods have been exploited to detect the concentration of phenolic compounds, including quartz crystal microbalance, high-performance liquid chromatography, electrophoresis, surface plasmon resonance spectroscopy, etc. [4] Although these methods can offer precise detection results of phenolic compounds, the analysis process is complicated and time-consuming, and the analysis machines are usually ponderous. Notably, enzyme-based electrochemical biosensor could effectively solve the above problems, attributing to its merits including fast response, low cost, high sensitivity, simple detection process, and no pre-treatment of samples [5]. To the best of our knowledge, a majority of electrochemical biosensors utilized modified electrodes (like glassy carbon electrode) as working electrode, free-standing electrodes especially flexible membrane electrode are rarely employed to directly detect phenolic compounds.

In addition, various approaches including physical, chemical, and biological methods have been applied in the removal of phenolic compounds, such as photo-Fenton oxidation, solvent extraction, ion exchange, electrochemical detoxification, biological treatment, etc. [6,7] Among these methods, biological methods have aroused wide attention due to the advantages of eco-friendly, high efficiency and safety [8,9]. Especially for approaches involving biological enzymes, which are not only efficiency in catalytic degradation, but also exhibit gradual decline in costs [10]. However, free enzymes tend to lose their activity during the procedure of application. In addition, the reuse of enzymes is also an unsolved challenge. To address the above problems, immobilization of enzymes has become a popular research topic [11].

Metal-organic framework (MOF) is a sort of porous hybrid material with metal-based nodes and organic links. Attributed to the large specific area, high porosity and tunable pore structures of MOF materials [12–14], they have been widely employed as matrix to immobilize various biological macromolecules, for instance DNA [15], enzymes [16,17], and drugs [18]. Therefore, the MOF-based composites are widely applied in sensors [19], catalysis [20], and drug delivery [18].

Recently, studies demonstrate that MOF is a satisfactory matrix for enzymes immobilization, because it can protect enzymes against the external environment, and the immobilization by MOF is even beneficial for enhancing the biological activity of enzyme [21–23]. Nevertheless, the recycling and reutilization of MOF-enzyme composites are still facing enormous challenges and difficulties. This is due to the fact that MOF materials are usually in powder form, which makes them easily dispersed in water and hard to collect. If MOF can be made into the form of continuous membrane materials, the recycle problem can be solved. Therefore, MOF-based membrane material is a good choice for the reuse of MOF-enzyme biocatalysts. Bacterial cellulose (BC) is an environment friendly fibrous material with high flexibility, strong strength, and excellent biocompatibility [24]. Combination of MOF and BC not only endows MOF flexible substrate but also maintains the intrinsic properties of MOF.

In this work, laccase (LAC) was selected as the biocatalytic enzyme because of its excellent catalysis towards phenolic compounds. ZIF-90 was chosen as the MOF material due to its good hydrophilicity. First of all, two types of ZIF-90-LAC composites were prepared to compare the enzyme activities of different immobilization strategies. After that, LAC@ZIF-90 composites were combined with BC and c-MWCNTs to prepare a flexible biocatalytic membrane. The novel membrane displayed its excellent detection and catalytic degradation effects towards catechol, a kind of phenolic compound. The membrane could be directly applied as biosensor electrode to detect catechol in river water. Moreover, the membrane could also be employed as a filtration membrane in enzyme membrane reactor (EMR) for degradation of catechol. In brief, a novel biocatalytic membrane was prepared and it could not only detect but also degrade phenolic compounds, which will find its potential application in simultaneous detection and degradation of phenolic pollutants in water environment.

2. Experimental

2.1. Materials

LAC (activity $\geq$ 50 units/mg) was obtained from Sigma Aldrich Chemical Co., Ltd. (St. Louis, MO, USA). BC was obtained from Jiangnan University, China. c-MWCNTs was obtained from Nanjing XFNANO Materials Tech Co. Ltd. Besides, zinc nitrate, imidazole-2-carboxaldehyde (ICA), polyvinyl pyrrolidone (PVP), catechol were purchased from Aladdin Chemical Reagent Co. Ltd (Shanghai, China). All the chemicals were used as received without further purification.

2.2. Synthesis method for LAC@ZIF-90 and LAC-ZIF-90

Scheme 1 shows the schematic synthesis process of LAC@ZIF-90 and LAC-ZIF-90.

LAC@ZIF-90 was synthesized as follows: ICA (480.0 mg) and PVP (50.0 mg) were added into deionized (DI) water (25 mL). To obtain a clear solution, the mixture was dissolved at 80 °C for 4 h. After the solution cooled to room temperature, 0.6 mL (1 g/L) of LAC was rapidly added to this solution in a static state for 10 min. Then, 6 mL zinc nitrate solution containing 742.6 mg of zinc nitrate was added in the solution. The mixture solution was kept a static state for a few minutes. Finally, the precipitate was collected by centrifugation (10,000 g) and washed with DI water for 3 times. Thus the LAC@ZIF-90 were obtained.

LAC-ZIF-90 was synthesized as follows: zinc nitrate (371.3 mg) was added into DI water (3 mL). Simultaneously, ICA (480.0 mg) and PVP (50.0 mg) was dissolved in DI water (25 mL) at elevated temperature. After mixing the solutions above for a few minutes, the precipitate was collected and washed by DI water. The obtained ZIF-90 was immersed in the LAC solution (1 g/L) for 15 min. The LAC-ZIF-90 were achieved by centrifugation and washed with DI water.

2.3. Preparation of BC/c-MWCNTs/LAC@ZIF-90 biocatalytic membrane

The preparation process of BC/c-MWCNTs/LAC@ZIF-90 biocatalytic membrane was depicted in Scheme 2. The whole process was simple and expected to achieve scalable production. Firstly, 500 mg of BC was processed into cellulose nanofibers slurry using a homogenizer. Then, 200 mg of c-MWCNTs, 100 mg of LAC@ZIF-90, and 100 mg of cetyltrimethyl ammonium bromide (CTAB, as dispersant) were added into the BC slurry to form a mixture solution. Lastly, the mixture solution was disposed by vacuum filtration utilizing a filter paper as supporting layer, the

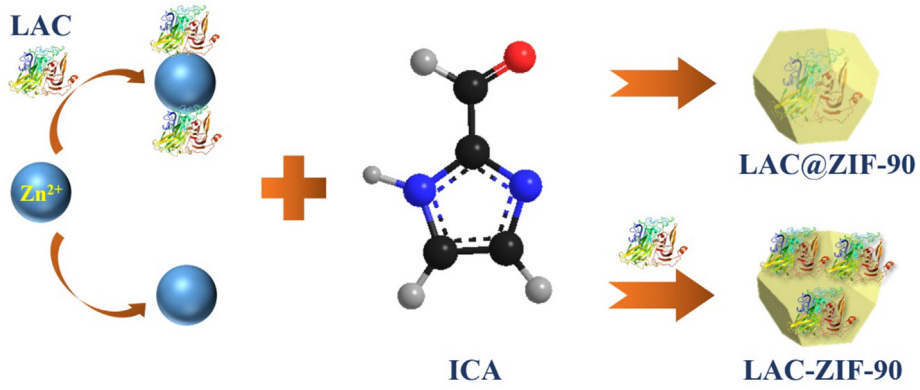

Scheme 1. Schematic synthesis process for LAC@ZIF-90 and LAC-ZIF-90.

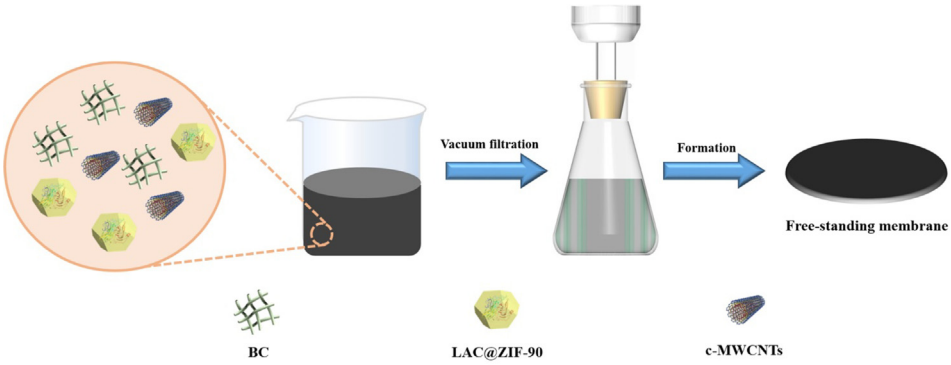

Scheme 2. Schematic preparation process for BC/c-MWCNTs/LAC@ZIF-90 membrane.

BC/c-MWCNTs/LAC@ZIF-90 biocatalytic membrane was finally obtained by separate the membrane on the surface of filter paper.

2.4. Materials characterization and measurements

The detailed materials characterization and measurements could be found in supplementary material.

3. Result and discussion

3.1. Characterization of LAC/ZIF-90 composites

3.1.1. Morphology characterization

ZIF-90 and LAC@ZIF-90 composites were observed by scanning electron microscopy (SEM). As shown in Fig. 1a and b, ZIF-90 and LAC@ZIF-90 possessed the same truncated cubic crystals structures, with an average diameter of ca. 2 μm, which is in consistent with that reported in literature [21]. For further confirming the immobilization of LAC by ZIF-90 crystal and evaluating the presence and spatial distribution of LAC in (or on) the ZIF-90, the LAC/ZIF-90 bio-composites were examined using confocal laser microscopy (CLSM). LAC-ZIF-90 and LAC@ZIF-90 show a different enzyme spatial distributions in Fig. 1c and Fig. 1d (also see in Fig. S1). The LAC molecules were mainly determined on the surfaces of the LAC-ZIF-90 composites, while the LAC molecules were evenly dispersed throughout LAC@ZIF-90 [25], which demonstrated that the LAC was well immobilized on (or in) the ZIF-90, and the morphology structures of the ZIF-90 crystals were not damaged.

3.1.2. Structure analysis

UV–visible spectra was employed to investigate the basic structure changes of the LAC and the LAC/ZIF-90 composites. As shown in Fig. S2a, a UV-absorption peak of the protein were depicted at 229 nm, attributing to the absorption peak of peptide group, which was coincident with the peak position in previous studies. LAC-ZIF-90 and LAC@ZIF-90 show the same absorption peaks with the free LAC, indicating that the basic structure of the LAC on (or in) ZIF-90 maintained unchangeable.

Fig. 2a shows the fluorescence spectroscopy of ZIF-90, free LAC, and LAC/ZIF-90 bio-composites. Since the fluorescent emission products of tryptophan derivatives (Trp −14, −142, −182, −185, −276 and −302) are sensitive to environmental, the fluorescence of tryptophan is usually used to explore the conformational change of LAC. As is depicted in Fig. 2a, the emission files of LAC-ZIF-90 and LAC@ZIF-90 is basically consistent with the free LAC. (λ_{max} = 333 nm) [21]. It can be considered that the tertiary structure of the LAC was not destructed, whether the LAC is immobilized on or inside the ZIF-90 particles.

3.1.3. XRD, FTIR, BET, and TGA analysis

X-Ray diffraction (XRD) was employed to study the crystal structure of ZIF-90. In XRD spectra (Fig. 2b), the positions and intensities of diffraction peaks of the synthesized ZIF-90 are consistent with the previous reports [26,27], revealing the successful formation of ZIF-90. The diffraction peaks at 2θ from left to right are X-ray reflections from (011), (200), (112), (022), (013), (222), (114), (233) and (134) planes of crystal structure which corresponding appeared in 7.6°, 10.6°, 12.9°, 14.9°, 16.6°, 18.2°, 22.3° and 26.8°. After combining with LAC, the position of the major

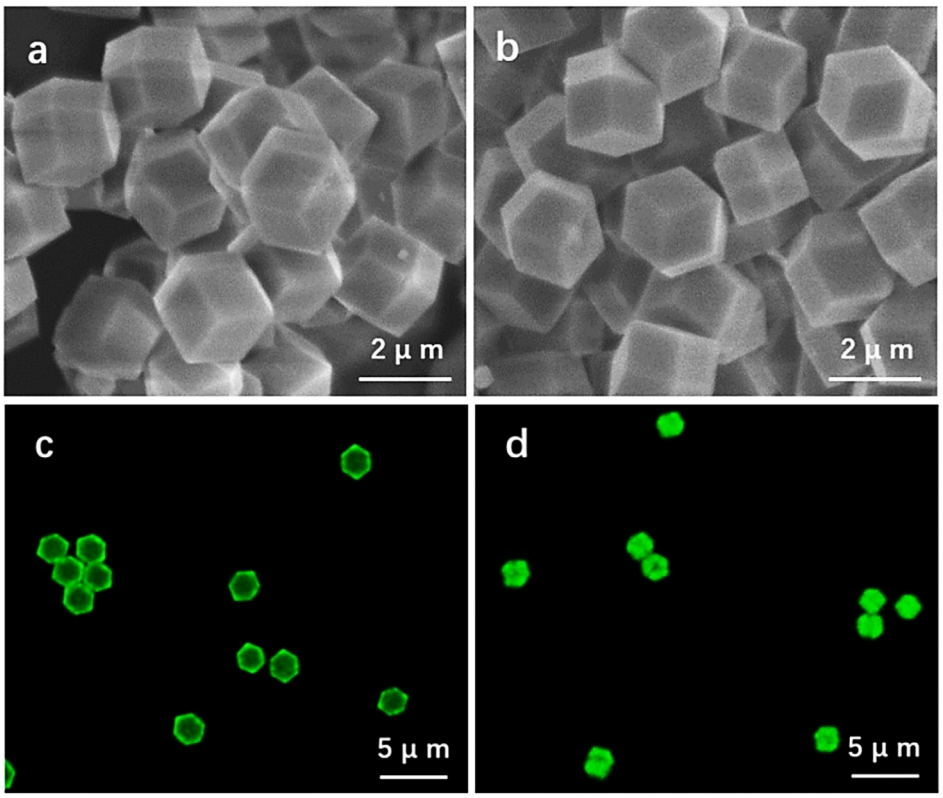

Fig. 1. SEM images of (a) ZIF-90 and (b) LAC@ZIF-90, CLSM images of (c) LAC-ZIF-90 and (d) LAC@ZIF-90.

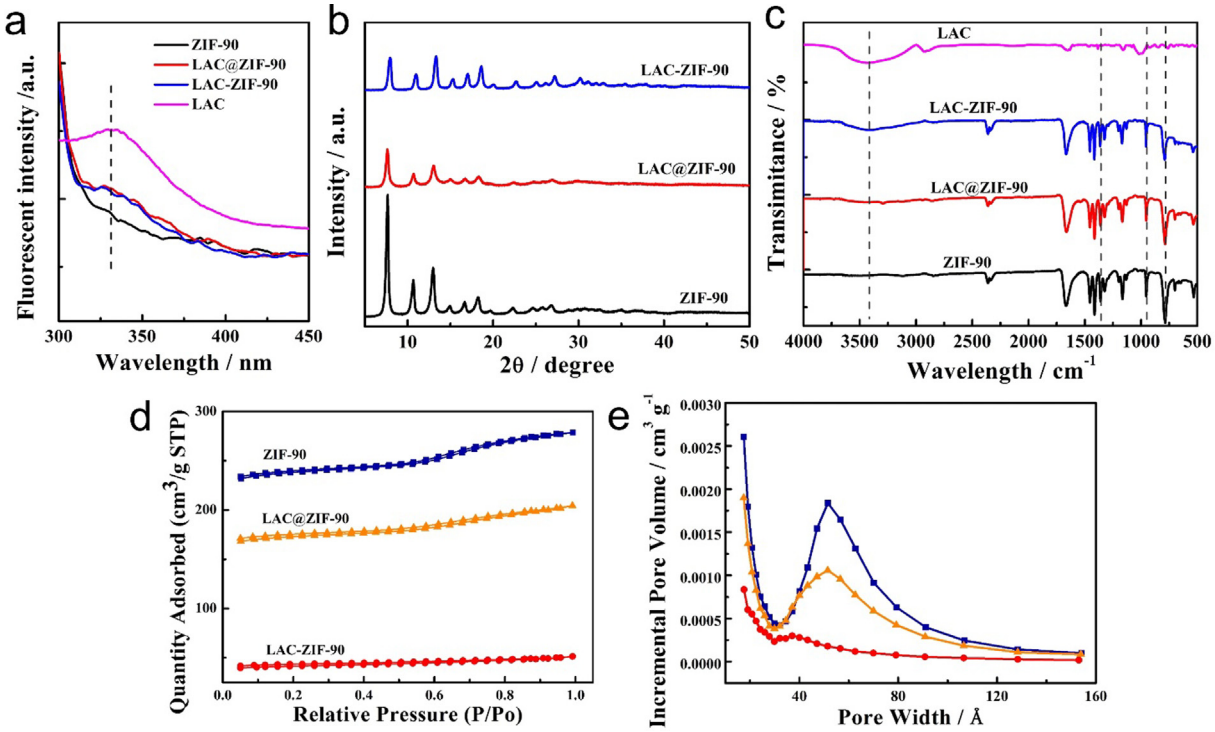

Fig. 2. (a) Fluorescence spectroscopy of LAC, ZIF-90, LAC-ZIF-90, and LAC@ZIF-90; (b) XRD patterns of ZIF-90, LAC-ZIF-90, and LAC@ZIF-90; (c) FT-IR spectra of LAC, ZIF-90, LAC-ZIF-90, and LAC@ZIF-90; (d) Nitrogen adsorption–desorption isotherm and (e) Pore size distribution curves of ZIF-90, LAC@ZIF-90, and LAC-ZIF-90.

diffraction peaks of LAC-ZIF-90 and LAC@ZIF-90 bio-composites showed almost no change. While, the intensity is reduced, which may be ascribed to a change in composition or blowhole blockage resulted by the combination of LAC and ZIF-90. All in all, the diffraction peaks of LAC-ZIF-90 and LAC@ZIF-90 demonstrate that there are no obvious change in ZIF-90 crystal and structure.

The FTIR spectra of pure LAC, ZIF-90, LAC-ZIF-90, and LAC@ZIF-90 are shown in Fig. 2c. In the pure ZIF-90 crystal, the bands at 600–1500 cm^{-1} are caused by the entire ring stretching or bending. The peaks at 954 cm^{-1} and 785 cm^{-1} are respectively attributed to the in-plane and out-of-plane bending of imidazole ring [28,29]. Besides, a band which appears at 1360 cm^{-1} accounts for the C—N stretching vibration of the imidazole moieties. Specifically, due to the C═O stretching, there is a characteristic peak at 1667 cm^{-1}, which could provide further evidence for aldehyde groups present in ZIF-90 crystals [302827]. It is worth noting that a new peak at 3440 cm^{-1} appears in the spectra of LAC-ZIF-90 and LAC@ZIF-90 composites, while the peak could not be seen in the ZIF-90 spectrum. Therefore, It could be considered that the hydroxyl groups take effect, simultaneously, it reflected the spectrum of LAC after protein immobilization. In addition, the peak of LAC-ZIF-90 was more obvious than that of LAC@ZIF-90, since the LAC molecules were distributed on the surface region for LAC-ZIF-90. The above results demonstrate that LAC has been successfully loaded by ZIF-90.

The pore textural properties of ZIF-90 were determined by N_2 adsorption isotherm in Fig. 2d and Fig. 2e. According to the International Union of Pure and Applied Chemistry (IUPAC) classification, the corresponding isotherm of ZIF-90 is identified as type I isotherm. The results (see Table 1) exhibited that the BET surface area of ZIF-90 was 721.49 $m^2\ g^{-1}$, indicating the excellent adsorption capacity of ZIF-90. According to the density functional theory (DFT), the pore volume of the mesoporous cage was 0.338 $cm^3\ g^{-1}$ and the pore diameter of ZIF-90 was 46.218 Å. Primarily, the residual porosity after enzyme immobilization varies with the immobilization strategies. While, the BET specific surface area of LAC-ZIF-90 composite material was significantly decreased to 123.41 $m^2\ g^{-1}$, which was caused by that the external pores of ZIF-90 was blocked by LAC. Notably, the BET specific surface area of LAC@ZIF-90 was slightly decreased to 526.62 $m^2\ g^{-1}$. Actually, the LAC in the pores of ZIF-90 occupies parts of the pore volumes. Therefore, the pore volume of LAC-ZIF-90 reduced significantly, while that of LAC@ZIF-90 decreased mildly. Because the larger BET surface area and pore size of ZIF-90 were beneficial to adsorption and catalysis of phenolic pollutant, LAC@ZIF-90 was more suitable for preparation of biocatalysis membrane in the following experiments.

Fig. S2b shows TGA curves of ZIF-90, LAC-ZIF-90, and LAC@ZIF-90. For ZIF-90, an initial weight loss occurred among the temperature range 50–320 °C, attributing to the exclusion of unreacted species (such as water and DMF molecules) that trapped in the pores of ZIF-90 [31]. The second weight loss from 320 to 800 °C was caused by the collapse of framework structure of ZIF-90 [32]. Notably, the remaining weight percentage of ZIF-90 at 800 °C was 58.2%, while that of LAC@ZIF-90 at 800 °C was only 52.3%, corresponding to the decomposition of LAC molecules. Thus, the TGA results demonstrated the successful immobilization of LAC in ZIF-90.

3.2. Comparison of free LAC, LAC-ZIF-90, and LAC@ZIF-90

3.2.1. Kinetics analysis

Michaelis-Menten kinetic was employed to fit the oxidation kinetics of ABTS by free LAC, LAC-ZIF-90, and LAC@ZIF-90, respectively. As is shown in Table 2, the immobilization amount of LAC for LAC@ZIF-90 is 107.83 mg g^{-1}, which is almost double of that for LAC-ZIF-90, indicating the higher immobilization capacity by encapsulation method. Besides, the V_{max} value and K_m value of free LAC were 8.73 μmol min^{-1} and 0.68 mM, respectively. While, for LAC-ZIF-90, the V_{max} value was decreased to 3.67 μmol min^{-1}, the K_m value increased to 2.37 mM. This phenomenon may be caused by the restricted substrate diffusion by LAC-ZIF-90. Nevertheless, these two values changed slightly for LAC@ZIF-90, which were 7.11 μmol min^{-1} and 0.82 mM, respectively. This result suggested that the substrate diffusion occurred smoothly in LAC@ZIF-90.

3.2.2. Stability of LAC, LAC-ZIF-90, and LAC@ZIF-90

In order to investigate the protection function of ZIF-90 for LAC, the influences of different temperatures on LAC activity were compared, the results are shown in Fig. 3a. As the environmental temperature increased from 50 to 70 °C, the residual activity of LAC declined apparently. It is noticeable that the activity of LAC for LAC@ZIF-90 was much higher than those of free LAC and LAC-ZIF-90, even at 70 °C, it still remained an above 60% of activity, demonstrating that the ZIF-90 could effectively protect the inside LAC against high temperature. Fig. 3b shows the effects of various organic solvents on the activity of LAC. Likewise, the LAC of LAC@ZIF-90 displayed the highest residual activity than the free LAC and LAC-ZIF-90, suggesting that ZIF-90 protective layer could help LAC against the influence of organic solvent. In addition, the storage stability and recyclability of LAC, LAC-ZIF-90, and LAC@ZIF-90 were also studied. It can be seen from Fig. 3c, the LAC@ZIF-90 showed apparently higher residual activity as comparison with free LAC and LAC-ZIF-90. Even through 30 days of storage, the LAC in LAC@ZIF-90 could maintained above 80% of initial enzyme activity, indicating the excellent storage stability of LAC@ZIF-90. Meanwhile, the LAC@ZIF-90 exhibited better recyclability than LAC-ZIF-90, LAC@ZIF-90 still retained over 80% of activity while the activity of LAC-ZIF-90 has been decreased to only 46% of initial activity after 8 cycles. Based on the above research, the LAC@ZIF-90 demonstrated its outstanding stability, hence we used LAC@ZIF-90 to prepare conductive biocatalysis membrane in the following experiments.

3.3. Characterization of BC/c-MWCNTs/ LAC@ZIF-90 membrane

3.3.1. Morphology characterization

Fig. 4a shows the photo of as-prepared BC/c-MWCNTs/LAC@ZIF-90 membrane, which is a black and free-standing circular membrane. Meanwhile, this membrane is flexible, as shown in Fig. 4b.

Table 2
Kinetic profile of free LAC, LAC-ZIF-90, and LAC@ZIF-90.

Sample	Immobilization amount (mg g^{-1})	V_{max} (μmol min^{-1})	K_m (mM)
LAC		8.73	0.68
LAC-ZIF-90	52.31	3.67	2.37
LAC@ZIF-90	107.83	7.11	0.82

Table 1
Porous characteristic of free LAC, LAC-ZIF-90, and LAC@ZIF-90.

Particles	BET Surface area ($m^2\ g^{-1}$)	Langmuir surface area ($m^2\ g^{-1}$)	Pore volume ($cm^3\ g^{-1}$)	Pore size (Å)
ZIF-90	721.49	1104.66	0.338	46.218
LAC-ZIF-90	123.41	199.81	0.054	38.030
LAC@ZIF-90	526.62	802.79	0.244	44.410

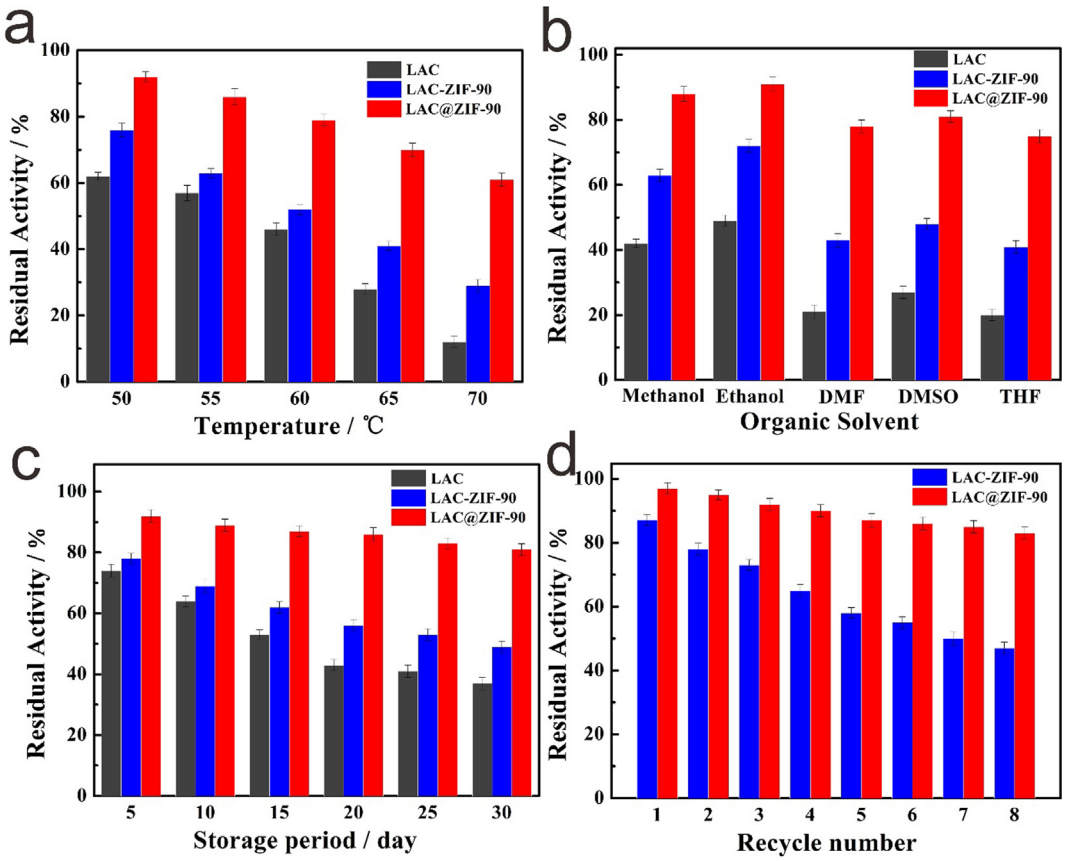

Fig. 3. (a) Thermal stability, (b) Organic solvent stability, (c) Storage stability of free LAC, LAC-ZIF-90, and LAC@ZIF-90; (d) Recyclability of LAC-ZIF-90 and LAC@ZIF-90.

Fig. 4c and 4d displays the SEM images of pure BC nanofibers and BC/c-MWCNTs/LAC@ZIF-90, respectively. The BC nanofibers were formed by randomly distributed ultrafine fibers with average diameter of ca. 30 nm. And the c-MWCNTs and LAC@ZIF-90 were well combined with BC nanofibers, which can be seen from Fig. 4d. Besides, according to the EDS results (see Fig. 4e and 4f), it is manifested that the content of C element of BC/c-MWCNTs/LAC@ZIF-90 membrane was much more than that of BC/LAC@ZIF-90 membrane, also demonstrating the existence of c-MWCNTs.

3.3.2. EDS, XPS, and TGA analysis

The surface elements of BC/c-MWCNTs/LAC@ZIF-90 membrane were characterized by EDS and XPS. Fig. 5 depicts the SEM-EDS elemental mapping images of BC/c-MWCNTs/LAC@ZIF-90, the C, N, O, and Zn elements were uniformly distributed on the whole membrane surface, suggesting the homogeneous distribution of LAC@ZIF-90 in composite membrane.

Fig. 6a exhibits the XPS spectra of BC, BC/LAC@ZIF-90, and BC/c-MWCNTs/LAC@ZIF-90. It is manifest that the BC/c-MWCNTs/LAC@ZIF-90 shows Zn2p peaks compared with pure BC. These two peaks were located at 1023 and 1046 eV, corresponding to Zn $2p_{3/2}$ and Zn $2p_{1/2}$, respectively (see Fig. 6b) [33]. The XPS characterization also demonstrated the existence of LAC@ZIF-90 in the membrane. Fig. 6c shows the TGA curves of BC, BC/LAC@ZIF-90, and BC/c-MWCNTs/LAC@ZIF-90. For BC, the initial weight loss occurred between 30 and 100 °C, ascribed to the evaporation of water. After that, there were two stages of weight variations that 100–320 °C and 320–600 °C, respectively, which could be corresponded to the typical degradation of cellulose chains. It is noticeable that the residue weight of BC/c-MWCNTs/LAC@ZIF-90 at 800 °C was larger than that of BC/LAC@ZIF-90, much more than that of pure BC. Moreover, the maximum thermal decomposition speed also displayed obvious difference (see Fig. 6d). On the one hand, c-MWCNTs and ZIF-90 were hard to thermal degradation; on the other hand, they also enhanced the thermal stability of BC nanofibers.

3.4. Biosensor application of BC/c-MWCNTs/LAC@ZIF-90 membrane

3.4.1. Electrochemical characterization of BC/c-MWCNTs/LAC@ZIF-90

Electrochemical Impedance Spectroscopy (EIS) was employed to investigate the interface resistance of LAC, ZIF-90, c-MWCNTs/LAC@ZIF-90, and BC/c-MWCNTs/LAC@ZIF-90 modified electrodes, and the results are illustrated in Fig. 7a. The semicircle diameters of the EIS plots reflect the electron transfer resistance of the electrochemical reaction (Ret), i.e. interface resistance. Apparently, LAC and MOF modified electrodes exhibited relatively high interface resistance due to their poor conductivity. Nevertheless, the c-MWCNTs/LAC@ZIF-90 and BC/c-MWCNTs/LAC@ZIF-90 modified electrodes showed much lower interface resistance (see Fig. S3), which could be attributed to the excellent conductivity of c-MWCNTs.

Fig. 7b compares the CVs of different electrodes in 300 μM of catechol solution. Herein, BC/LAC@ZIF-90 and BC/c-MWCNTs/LAC@ZIF-90 free-standing membrane were directly used as working electrode. It can be clearly seen that the BC/c-MWCNTs/LAC@ZIF-90 membrane electrode displayed the largest anodic (E_{pa}) and cathodic (E_{pc}) peak currents compared with other three electrodes, indicating the optimal electrocatalysis towards catechol. Besides, as shown in Fig. 7c, the anodic and cathodic peak cur-

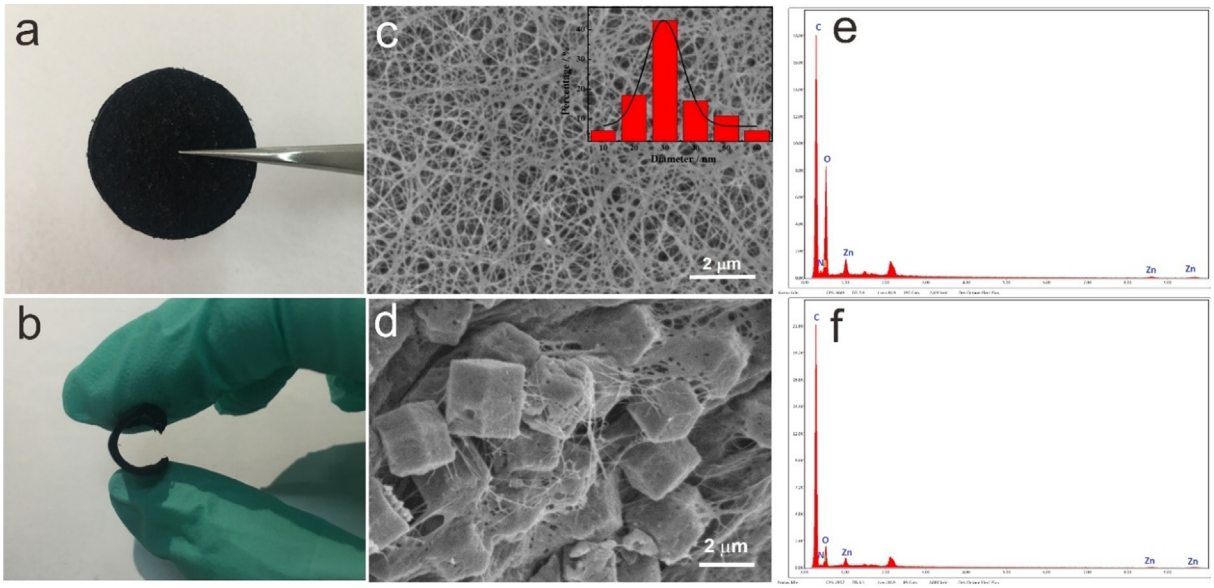

Fig. 4. (a) Photo of as-prepared BC/c-MWCNTs/LAC@ZIF-90 membrane; (b) Flexural display of BC/c-MWCNTs/LAC@ZIF-90 membrane; SEM images of (c) pure BC nanofibers (inset: diameter distribution of nanofibers) and (d) BC/c-MWCNTs/LAC@ZIF-90 membrane; EDS of (e) BC/LAC@ZIF-90 membrane, and (f) BC/c-MWCNTs/LAC@ZIF-90 membrane.

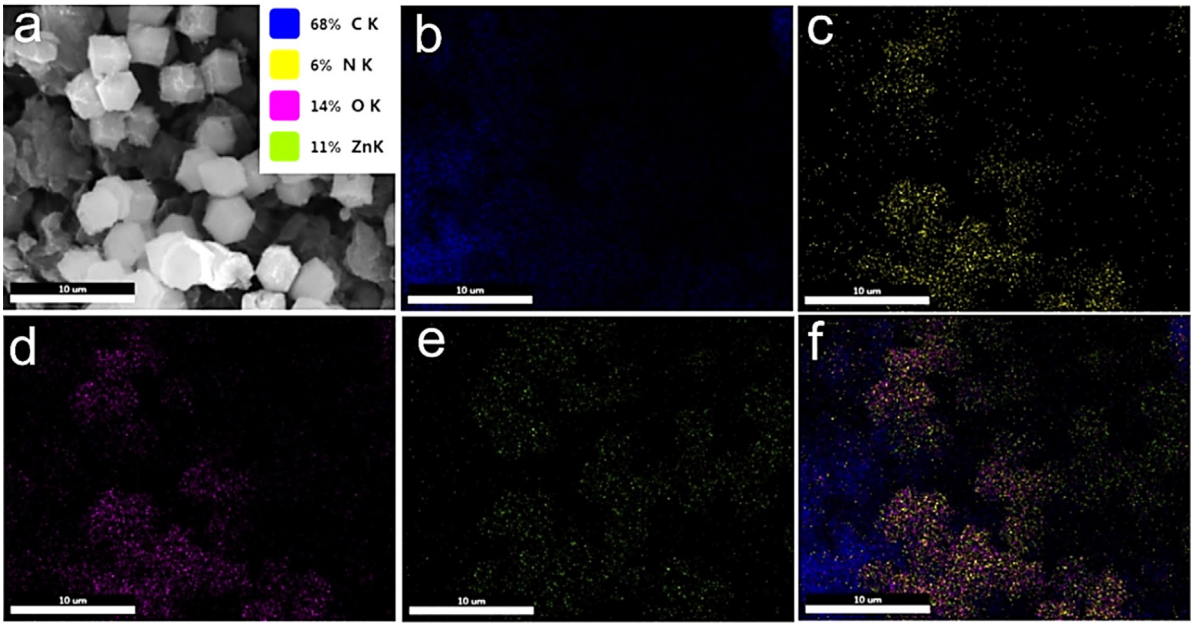

Fig. 5. SEM-EDS elemental mapping images of BC/c-MWCNTs/LAC@ZIF-90 membrane: (a) Original image; (b) C mapping; (c) N mapping; (d) O mapping; (e) Zn mapping; (f) Overlap mapping.

rents increased simultaneously with the increase of scan rates from 10 to 90 mV/s. Moreover, the current change values were proportional to the scan rates according to the fitting plot in the inset of Fig. 7c, suggesting that the whole electrochemical process was a surface-controlled redox process. Moreover, the E_{pa} and E_{pc} peak potentials changed to more positive and more negative values, respectively, suggesting that the electrochemical reaction process was a quasi-reversible process. Fig. 7d depicts the influence of solution pH on the CV curve of BC/c-MWCNTs/LAC@ZIF-90. It can be seen that the whole curves shifted to left as pH changed from 3 to 6. The largest anodic peaks current was 20.86 μA when pH was 4. Therefore, pH 4 was selected as the optimum pH in the following differential pulse voltammetry (DPV) tests.

3.4.2. Catechol detection by BC/c-MWCNTs/LAC@ZIF-90 membrane electrode

DPV was employed to determine the concentration of catechol in acetate buffer (0.2 M, pH 4), the result is shown in Fig. 7e. Obviously, as the catechol concentration enhanced from 20 to 400 μM, the DPV peak currents increased simultaneously. The calibration curve of DPV peak currents *vs.* catechol concentration was displayed in Fig. 7f. The linear equation was I = 86.96 + 22C, r^2 = 0.9938, where I is the peak current in μA and C is the concentration in μM. The sensitivity was as high as 22 μA/mM and the detection limit (S/N = 3) was 1.86 μM. The performance of BC/c-MWCNTs/LAC@ZIF-90 based biosensor was compared with other LAC based biosensors, as shown in Table S1. Our sensor possessed

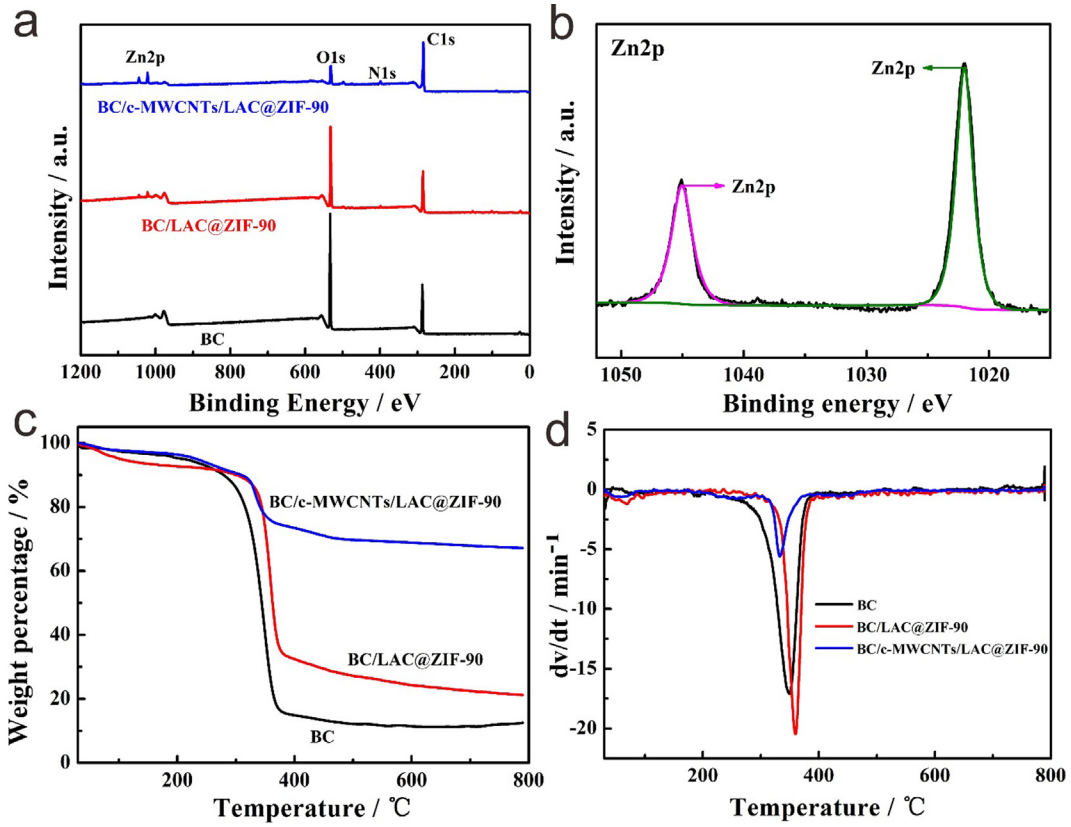

Fig. 6. XPS spectra (a), TGA curves (c), DTG curves (d) of BC, BC/LAC@ZIF-90, and BC/c-MWCNTs/LAC@ZIF-90; (b) High-resolution Zn 2p peaks of BC/c-MWCNTs/LAC@ZIF-90.

satisfactory detection limit and wide linear range, implying its application potential in the field of phenolic compounds detection.

The biocatalytic mechanism is displayed in Scheme 3. It can be seen that the conductive membrane electrode was consisted by BC, c-MWCNTs, and LAC@ZIF-90. The BC offered a flexible membrane substrate, c-MWCNTs enabled the membrane conductive, and the LAC@ZIF-90 could catalyzed the phenolic compounds. The catechol on contact with the LAC embedded in ZIF-90 was oxidized to 1,2-benzoquinone along with oxygen molecular reduced to H_2O. During this process, the electrons could transport through the c-MWCNTs, which could produce current response detected by electrochemical workstation.

3.4.3. Selectivity, reproducibility, stability, and real sample analysis of the biosensor

Selectivity is important for the application of biosensors. In this study, several sorts of phenolic compounds, including aminophenol, gallic acid, catechin, phenol, and hydroquinone were employed to investigate the selectivity of the biosensor via DPV. The peak currents were determined by the biosensor in 300 μM of catechol solution containing the interferents with 1:1 ratio. Through recording the response current before and after adding interferents, it can be found that every interferent almost not contributed to the sensor response (see Fig. S4), indicating the satisfactory selectivity of the biosensor.

In addition, the biosensor also showed great reproducibility, repeatability, and stability. Three BC/c-MWCNTs/LAC@ZIF-90 membrane were prepared by same conditions and the relative standard deviation (RSD) of the response of the three membrane biosensors towards catechol was only 2.3%, implying the good reproducibility of the biosensor. During 10 times of successive tests for catechol of one biosensor, the RSD was within 2%, demonstrating the great repeatability of the biosensor. Fig. S5 displays the storage stability of the biosensor at 4 °C, it was manifest that even through 30 days of storage, the sensor response still could maintained ca. 93.6% of the initial value. Thus, the biosensor possessed satisfactory storage stability.

Yangtze river water was chosen as real water sample to investigate the practical application of the biosensor. Herein, a recovery experiment with 5 times was employed, and the results are displayed in Table S2. It can be seen that the recoveries were satisfactory, demonstrating that the biosensor could meet the detection requirement in real water sample analysis.

3.5. Catechol degradation and EMR application

To investigate the degradation capacity of BC/c-MWCNTs/LAC@ZIF-90 membrane towards hazardous phenolic compounds, catechol was selected as object to compare the degradation effects of free and immobilized LAC. As shown in Fig. 8a, through 2 h of degradation, the degradation efficiency of free LAC towards catechol was 88.4%. Nevertheless, this value for BC/c-MWCNTs/LAC was decreased to 46.8%, indicating that the enzyme activity of LAC declined after immobilization on BC/c-MWCNTs membrane. Notably, the degradation efficiency of BC/c-MWCNTs/ LAC@ZIF-90 was as high as 93.4%, which proved the excellent degradation capacity of LAC@ZIF-90 towards catechol. It can be attributed to that the framework of ZIF-90 well protected the LAC to avoid reduction of enzyme activity. Meanwhile, the favorable adsorption role of ZIF-90 improved the capture property of composite membrane to catechol.

In addition, the recyclability of the LAC-modified membranes by 5 cycles were compared. As shown in Fig. 8b, the degradation rate of BC/c-MWCNTs/LAC was reduced to only 26.8%, almost half of initial value. While, BC/c-MWCNTs/LAC@ZIF-90 still maintained ca. 82.1% of degradation rate to catechol, only slight decline as

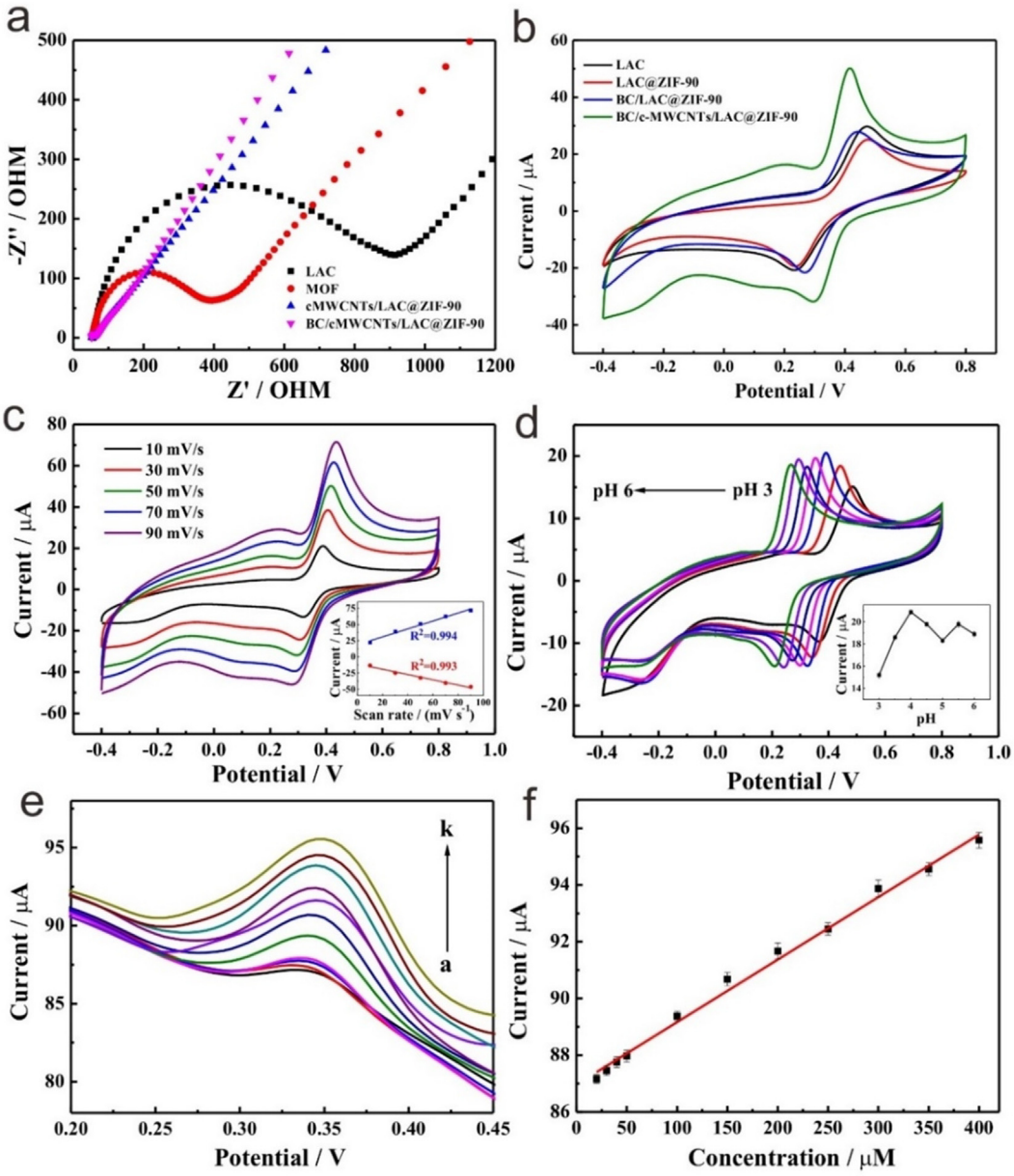

Fig. 7. (a) EIS of LAC, ZIF-90, cMWCNTs/LAC@ZIF-90, and BC/cMWCNTs/LAC@ZIF-90 electrodes; (b) CVs of LAC, LAC@ZIF-90, BC/ LAC@ZIF-90, and BC/cMWCNTs/LAC@ZIF-90 electrodes in 300 μM of catechol solution; (c) CVs of BC/cMWCNTs/LAC@ZIF-90 electrode at different scan rates from 10 to 90 mV/s (inset: plots of the corresponding anodic and cathodic peak currents *vs.* scan rate); (d) CVs of BC/cMWCNTs/LAC@ZIF-90 electrode by different pH from 3 to 6 (inset: plots of the oxidation peak current *vs.* pH); (e) DPVs of BC/cMWCNTs/LAC@ZIF-90 electrode towards different concentration of catechol from 20 to 400 μM; (f) Calibration curve of DPV peak currents *vs.* catechol concentration.

comparison with initial value. Thus, the BC/c-MWCNTs/LAC@ZIF-90 also possessed excellent reuse performance, displayed expected application potential in the field of phenolic wastewater treatment.

In order to evaluate the practical application of the membrane, we employed an enzyme membrane reactor (EMR) to investigate its degradation ratio towards catechol. As shown in Scheme 4 and Fig. S6, the reactor possesses a capacity of 500 mL, and the membrane with 8.0 cm of diameter was overlaid on a PS ultrafiltration membrane with same size to form the reaction layer. The catechol solution was added through a peristaltic pump with adjustable pressure, which utilized a N_2 regulator to control the flow rate. The filtrate was ejected from the outlet for the subsequent analyses.

As shown in Fig. 9a, when the operational pressure was enhanced from 20 to 200 Pa, the flux value of EMR was increased from 0.15 ± 0.02 to 0.83 ± 0.04 L m^{-2} min^{-1} (black curve), while the degradation ratio of catechol was declined from 91 ± 2.2% to 80 ± 2.9% (red curve). Therefore, the EMR could maintain a satisfactory degradation radio towards catechol even though the operational pressure and flux value were increased by several times. Moreover, the reusability of the EMR was studied, the result is shown in Fig. 9b. The removal rate of the EMR was analyzed once every day for 5 days (reaction time of 2 h) to examine the reusability. The initial removal rate was set as 100%, and the EMR still maintained ca. 72% of relative removal rate through 5 repeating cycles. In sum, the EMR based on the BC/c-MWCNTs/ LAC@ZIF-90

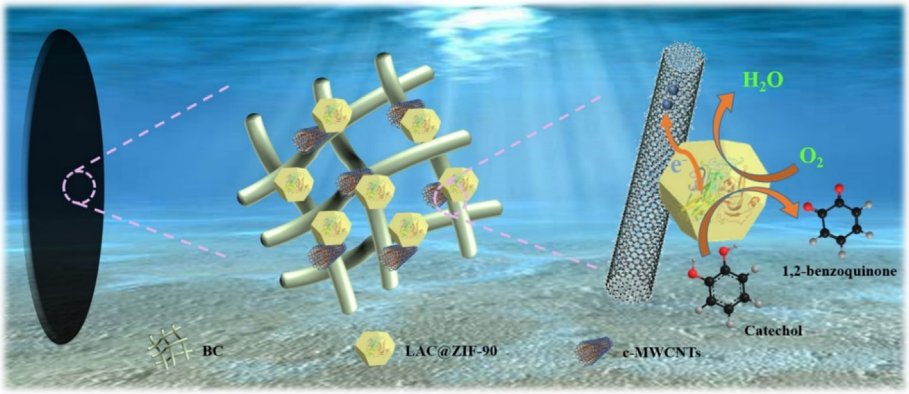

Scheme 3. Schematic illustration of the biocatalytic mechanism of the as-prepared membrane.

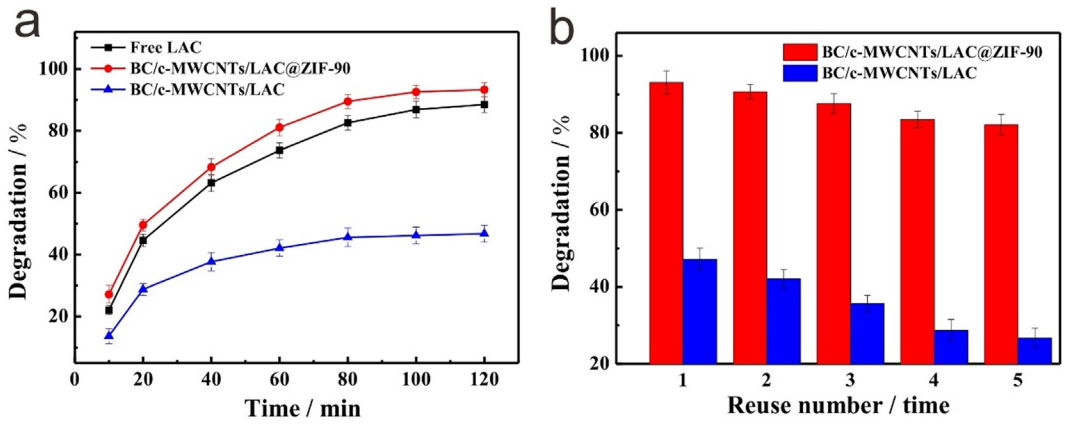

Fig. 8. (a) Removal efficiency of catechol by the free and immobilized LAC; (b) Recyclability of LAC-modified membrane by 5 cycles.

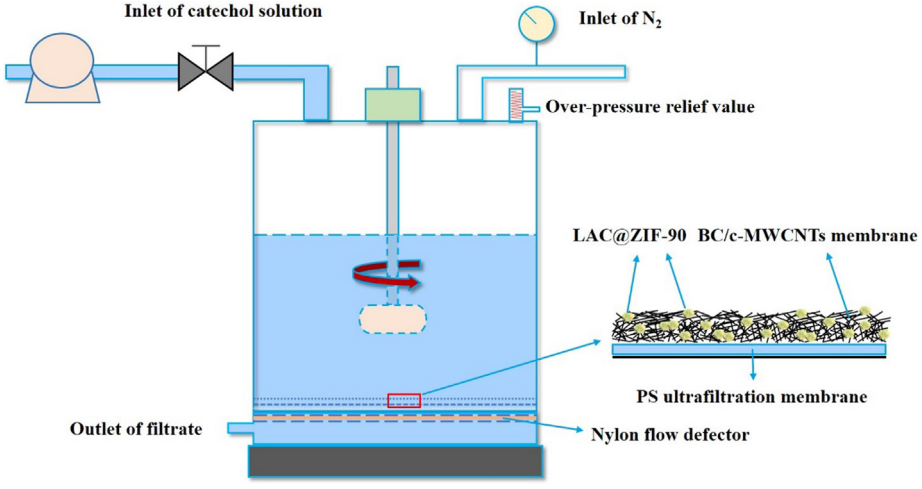

Scheme 4. Schematic diagram of the assembled EMR.

membrane possessed superior stability, catalysis efficiency, and reusability.

4. Conclusions

In summary, LAC was encapsulated in ZIF-90 to prepare LAC@ZIF-90 biocomposite. A bacterial cellulose-based biocatalytic membrane was prepared by combining LAC@ZIF-90, BC, and c-MWCNTs. The as-prepared BC/c-MWCNTs/LAC@ZIF-90 membrane showed excellent detection and degradation properties towards catechol. The membrane-based biosensor showed a linear response to catechol from 20 to 400 μM with a detection limit of 1.86 μM. Moreover, the membrane was successfully applied in EMR for the degradation of phenolic pollutant. Thus, the novel biocatalytic membrane will find its potential application on simultaneous monitor and degradation of phenolic wastewater.

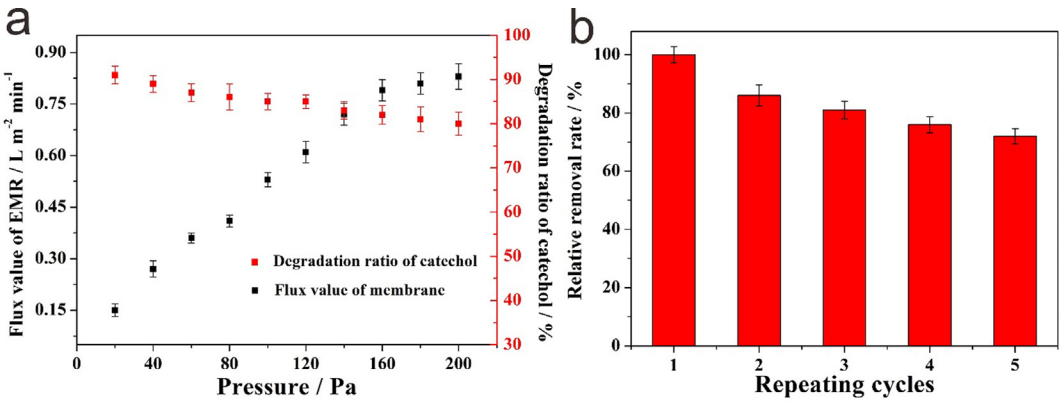

Fig. 9. (a) Degradation ratios of catechol under varied operational pressures; (b) Reusability of the EMR.

CRediT authorship contribution statement

Dawei Li: Methodology, Validation, Investigation, Data curation, Writing - original draft, Writing - review & editing. **Yue Cheng:** Investigation. **Han Zuov:** Investigation. **Wei Zhang:** Investigation. **Gangwei Pan:** Investigation, Writing - review & editing. **Yijun Fu:** Conceptualization, Software, Resources. **Qufu Wei:** Conceptualization, Software, Resources, Writing - review & editing, Supervision.

Declaration of Competing Interest

The authors declare that they have no known competing financial interests or personal relationships that could have appeared to influence the work reported in this paper.

Acknowledgements

This work was supported by the National Natural Science Foundation of China (51803078), the Natural Science Foundation of Jiangsu Province (BK20180628), the Nantong Science and Technology Project (MS12020074), the Natural Science Foundation of Jiangsu Province (BK20190927).

Appendix A. Supplementary data

Supplementary data to this article can be found online at https://doi.org/10.1016/j.jcis.2021.06.155.

References

[1] J. Liu, X. Shen, Z. Zheng, M. Li, X. Zhu, H. Cao, C. Cui, Immobilization of laccase by 3D bioprinting and its application in the biodegradation of phenolic compounds, Inter. J. Biol. Macromo. 164 (2020) 518–525.
[2] R. Mtibaà, D.R. Olicón-Hernández, C. Pozo, M. Nasri, T. Mechichi, J. González, E. Aranda, Degradation of bisphenol A and acute toxicity reduction by different thermo-tolerant ascomycete strains isolated from arid soils, Ecotox. Environ. Safe 156 (2018) 87–96.
[3] T. Doğan, E. Bayram, L. Uzun, S. Şenel, A. Denizli, Trametes versicolor laccase immobilized poly(glycidyl methacrylate) based cryogels for phenol degradation from aqueous media, J. Appl. Polym. Sci. 132 (20) (2015) 41981.
[4] S.R. Yashas, S. Sandeep, B.P. Shivakumar, N.K. Swamy, Potentiometric polyphenol oxidase biosensor for sensitive determination of phenolic micropollutant in environmental samples, Environ. Sci. Pollut. R. 27 (22) (2020) 27234–27243.
[5] T. Arfin, S.N. Rangari, Graphene oxide–ZnO nanocomposite modified electrode for the detection of phenol, Anal. Methods-Uk 10 (3) (2018) 347–358.
[6] E. Weidemann, M. Niinipuu, J. Fick, S. Jansson, Using carbonized low-cost materials for removal of chemicals of environmental concern from water, Energ. Convers. Manage. 25 (2018) 15793–15801.
[7] C.-G. Lee, H. Javed, D. Zhang, J.-H. Kim, P. Westerhoff, Q. Li, P.J.J. Alvarez, Porous electrospun fibers embedding TiO_2 for adsorption and photocatalytic degradation of water pollutants, Environ. Sci. Technol. 52 (7) (2018) 4285–4293.
[8] G.C. Wang, Y. Liu, M.H. Wu, W.J. Zong, X.L. Yi, J.J. Zhan, L.F. Liu, H. Zhou, Coupling the phenolic oxidation capacities of a bacterial consortium and in situ-generated manganese oxides in a moving bed biofilm reactor (MBBR), Water Res. 166 (2019) 11.
[9] K. Yuan, S. Li, F. Zhong, Treatment of coking wastewater in biofilm-based bioaugmentation process: Biofilm formation and microbial community analysis, J. Hazard. Mater. 400 (2020) 123117.
[10] J.B. Costa, M.J. Lima, M.J. Sampaio, M.C. Neves, J.L. Faria, S. Morales-Torres, A.P. M. Tavares, C.G. Silva, Enhanced biocatalytic sustainability of laccase by immobilization on functionalized carbon nanotubes/polysulfone membranes, Chem. Eng. J. 355 (2019) 974–985.
[11] D.-M. Liu, J. Chen, Y.-P. Shi, Advances on methods and easy separated support materials for enzymes immobilization, Trac-Trends Anal. Chem. 102 (2018) 332–342.
[12] Y. Luo, S. Fan, W. Yu, Z. Wu, D.A. Cullen, C. Liang, J. Shi, C. Su, Fabrication of $Au_{25}(SG)_{18}$–ZIF-8 nanocomposites:a facile strategy to position $Au_{25}(SG)_{18}$ nanoclusters inside and outside ZIF-8, Adv. Mater. 30 (2018) 1704576–1704579.
[13] A. Dhakshinamoorthy, S. Navalon, A.M. Asiri, H. Garcia, Metal organic frameworks as solid catalysts for liquid-phase continuous flow reactions, Chem. Commun. 56 (1) (2020) 26–45.
[14] F.G. Cirujano, A. Dhakshinamoorthy, Engineering of active sites in metal–organic frameworks for biodiesel production, Adv. Sustainable Syst. DOI: 10.1002/adsu.202100101.
[15] W. Morris, W.E. Briley, E. Auyeung, M.D. Cabezas, C.A. Mirkin, Nucleic acid–metal organic framework (MOF) nanoparticle conjugates, J. Am. Chem. Soc. 136 (20) (2014) 7261–7264.
[16] Y. Hu, L. Dai, D. Liu, W. Du, Y. Wang, Progress & prospect of metal-organic frameworks (MOFs) for enzyme immobilization (enzyme/MOFs), Renew. Sustain. Ener. Rev. 91 (2018) 793–801.
[17] A. Dhakshinamoorthy, A.M. Asiri, H. Garcia, Integration of metal organic frameworks with enzymes as multifunctional solids for cascade catalysis, Dalton Trans. 49 (32) (2020) 11059–11072.
[18] Y. Wang, J. Yan, N. Wen, H. Xiong, S. Cai, Q. He, Y. Hu, D. Peng, Z. Liu, Y. Liu, Metal-organic frameworks for stimuli-responsive drug delivery, Biomaterials 230 (2020) 119619.
[19] X. Fang, B. Zong, S. Mao, Metal–organic framework-based sensors for environmental contaminant sensing, Nano-Micro Lett. 10 (2018) 64.
[20] V. Pascanu, G. González Miera, A.K. Inge, B. Martín-Matute, Metal–organic frameworks as catalysts for organic synthesis: a critical perspective, J. Am. Chem. Soc. 141 (18) (2019) 7223–7234.
[21] W. Liang, H. Xu, F. Carraro, N.K. Maddigan, Q. Li, S.G. Bell, D.M. Huang, A. Tarzia, M.B. Solomon, H. Amenitsch, L. Vaccari, C.J. Sumby, P. Falcaro, C.J. Doonan, Enhanced activity of enzymes encapsulated in hydrophilic metal–organic frameworks, J. Am. Chem. Soc. 141 (6) (2019) 2348–2355.
[22] D. Feng, T.-F. Liu, J. Su, M. Bosch, Z. Wei, W. Wan, D. Yuan, Y.-P. Chen, X. Wang, K. Wang, X. Lian, Z.-Y. Gu, J. Park, X. Zou, H.-C. Zhou, Stable metal-organic frameworks containing single-molecule traps for enzyme encapsulation, Nat. Commun. 6 (2015) 5979.
[23] W.-H. Chen, M. Vázquez-González, A. Zoabi, R. Abu-Reziq, I. Willner, Biocatalytic cascades driven by enzymes encapsulated in metal–organic framework nanoparticles, Nat. Catal. 1 (2018) 1–7.
[24] W. Shao, J. Wu, H. Liu, S. Ye, L. Jiang, X. Liu, Novel bioactive surface functionalization of bacterial cellulose membrane, Carbohyd. Polym. 178 (2017) 270–276.
[25] F.-K. Shieh, S.-C. Wang, C.-I. Yen, C.-C. Wu, S. Dutta, L.-Y. Chou, J.V. Morabito, P. Hu, M.-H. Hsu, K.C.W. Wu, C.-K. Tsung, Imparting functionality to biocatalysts via embedding enzymes into nanoporous materials by a de novo approach: size-selective sheltering of catalase in metal–organic framework microcrystals, J. Am. Chem. Soc. 137 (2015) 4276–4279.

[26] P. Dr, S. Fa-Kuen, W. Shao-Chun, L. Sin-Yen, P. Dr, C.-W. Kevin, Water-based synthesis of zeolitic imidazolate framework-90 (ZIF-90) with a controllable particle size, Chem.-Eur. J. 19 (2013) 11139–11142.
[27] W. Xie, F. Wan, Guanidine post-functionalized crystalline ZIF-90 frameworks as a promising recyclable catalyst for the production of biodiesel via soybean oil transesterification, Energ. Convers. Manage. 198 (2019) 111922.
[28] D. Zhang, Y. Fan, G. Li, W. Du, R. Li, Y. Liu, Z. Cheng, J. Xu, Biomimetic synthesis of zeolitic imidazolate frameworks and their application in high performance acetone gas sensors, Sensor. Actuat. B-Chem. 302 (2020) 127187.
[29] M. Chai, A. Razmjou, V. Chen, Metal-organic-framework protected multi-enzyme thin-film for the cascade reduction of CO_2 in a gas-liquid membrane contactor, J. Membr. Sci. 623 (2021) 118986.
[30] M. Zhou, S. Dong, Bioelectrochemical interface engineering: toward the fabrication of electrochemical biosensors, biofuel cells, and self-powered logic biosensor, Acc. Chem. Res. 44 (2011) 1232–1243.
[31] T. Taghizadeh, A. Ameri, A. Talebian-Kiakalaieh, S. Mojtabavi, A. Ameri, H. Forootanfar, S. Tarighi, M.A. Faramarzi, Lipase@zeolitic imidazolate framework ZIF-90: A highly stable and recyclable biocatalyst for the synthesis of fruity banana flavour, Inter. J. Biol. Macromo. 166 (2021) 1301–1311.
[32] F.-K. Shieh, S.-C. Wang, S.-Y. Leo, K.-W. Wu, Water-based synthesis of zeolitic imidazolate framework-90 (ZIF-90) with a controllable particle size, Chem.-Eur. J. 19 (34) (2013) 11139–11142.
[33] Y. Cai, D. Chen, N. Li, Q. Xu, H. Li, J. He, J. Lu, Superhydrophobic metal–organic framework membrane with self-pepairing for high-efficiency oil/water emulsion separation, ACS Sustain. Chem. Eng. 7 (2019) 2709–2717.